Dust seminar week 3

Olivia Clifton

2/3/2016

Ch. 7 of textbook; Kok et al. 2014b

7.2 observational systems

long term in situ measurements of dust are rare over remote arid & semi arid regions prone to emissions, & oceanic regions affected by transport

- see Table 7.2 for examples of measurements for dust monitoring
- first available dust observations from synoptic meteorological stations based on visibility or dust weather code analysis
- recent measurements
  - in situ
    - only 3 sites in N. Atlantic & 1 in South Pacific w/ cts. obs. during last 20 years; many available datasets, especially over marine regions cover < 10 years; 3 ground-based cts. dust conc. measurement sites in Sahel started in 2006
      - dust load monitoring (mass concentrations) from various sampling systems (TEOM, filters)
        - this type of measurement indicates that regional & daily variability of sfc. dust loads is huge due to sporadic nature of dust events
  - remote sensing
    - ground based
      - AERONET, since mid-90s, global, key reference obs. system for aerosols
    - space based
      - > 20 separate satellite sensors available for aerosol studies
        - sun photometers: AOD, DOD
        - UV (TOMS OMI), IR (Meteosat,MSG): semi-quantitative indices used as proxies of dust events or loads, esp. over arid regions

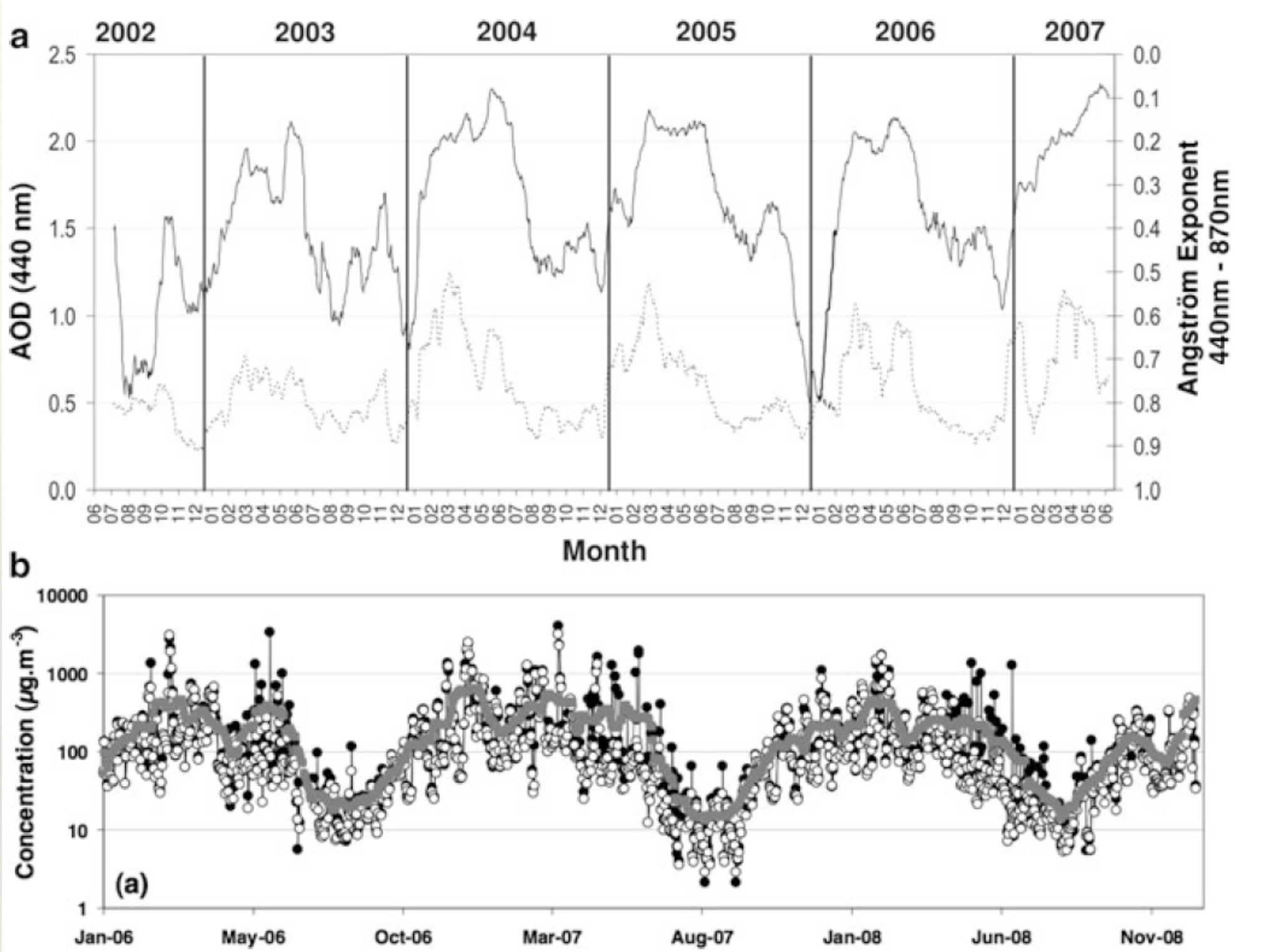

Fig. 7.1 Examples of multiyear measurements available for dust studies in West Africa at the station of Banizoumbou (Niger). (**a**) *AOD and Angström exponent*: 30-day sliding averages of daily AOD (440 nm, *dotted line*) and Angström exponent (440–870 nm, *solid line*) derived from the AERONET sun photometer for 2002–2007. From Rajot et al. (2008). (**b**) *PM10*: daily mean (*black circle*) and median (*open circle*) concentration and 30-day sliding average of the daily mean (*grey line*) from 2006 to 2008 (From Marticorena et al. 2010)

large variability of dust on daily and seasonal timescales!

source regions: regional data from geostationary satellites

- IDDI from Meteosat-I daily noontime IR images
  - over continental Africa, 1984-1993 [Brooks and Legrand 2000; Legrand et al. 2001]
    - seasonal and inter-annual variability
    - application: dust source ident. over Sahara & Sahel
  - 1 year (1999) over arid & semi-arid areas surrounding N. Indian Ocean [Léon and Legrand 2003]
- SEVIRI/MSG thermal IR radiance measurements [Schepanski et al. 2007]
  - N. African dust sources
  - observations of dust source activation; every 3 hours [Schepanski et al. 2009] => obtain diurnal cycles and investigate met. controls on dc
    - Schepanski et al. [2009] find that emissions peak in early morning due to breakdown of nocturnal low-level jets
  - no quantitative OD or source strength from this approach
    - however, approach of Banks and Brindley [2013] may allow for quantitative analysis of high temporal resolution (half-hourly) mineral dust source variability over N. Africa & Middle East

source regions: global data from polar-orbiting satellite

- AI from TOMS/Nimbus 7 measurements in UV [Herman et al. 1997]
  - first product used to identify & characterize mineral dust sources @ global scale [Prospero et al. 2002]
  - proxy for dust source ident.: regions w/ max. AI or high freq. of high AI occurrences
    - less sensitive to aerosols at low altitude => sometimes questionable dust source ident. [Mahowald and Dufresne 2004]
    - difficult to determine whether dust has been transported or emitted at the source
- Deep Blue algorithm from MODIS in the 412 nm channel [Hsu et al. 2004]
  - detect dust close to surface, high spatial res. (0.1°)
  - use size distribution & optical properties to go from AOD to DOD
  - dust retrieval is limited to bright surfaces => dust sources in n. high lats. may be underrepresented [Ginoux et al. 2012]

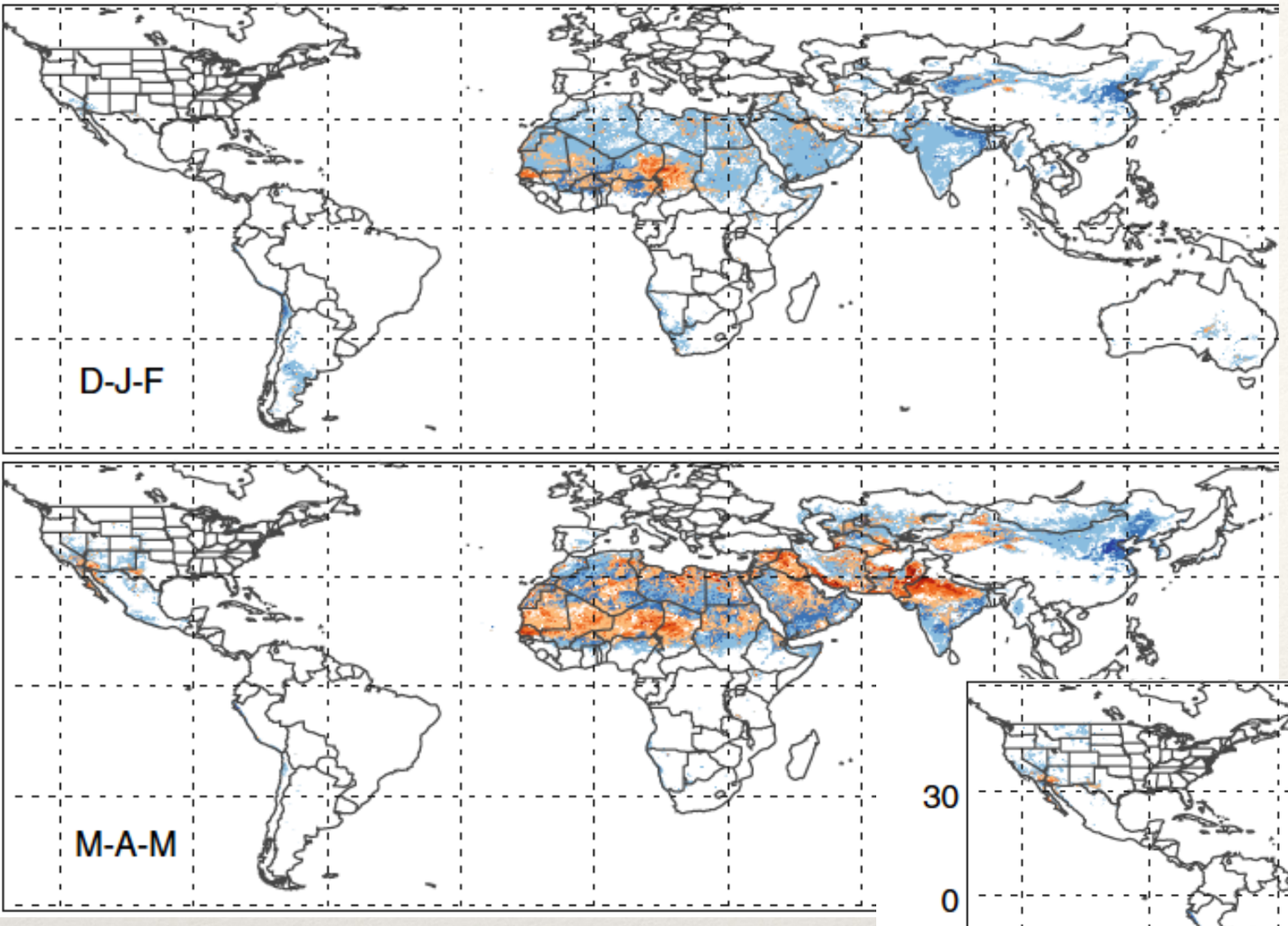

Fig. 7.2 Global distribution of MODIS Deep Blue seasonal mean AOD (blue) overplotted by DOD (red) at 550 nm, for values greater than 0.1. The retrieval is restricted to bright land surfaces. The data are from MODIS/Aqua at 0.1° x 0.1° resolution averaged over the period 2003–2009 (From Ginoux et al. 2012)

- remarkably little dust activity in the SH [Prospero et al 2002; Ginoux et al. 2012]
- highest DOD values occur during spring and summer over arid areas in NH

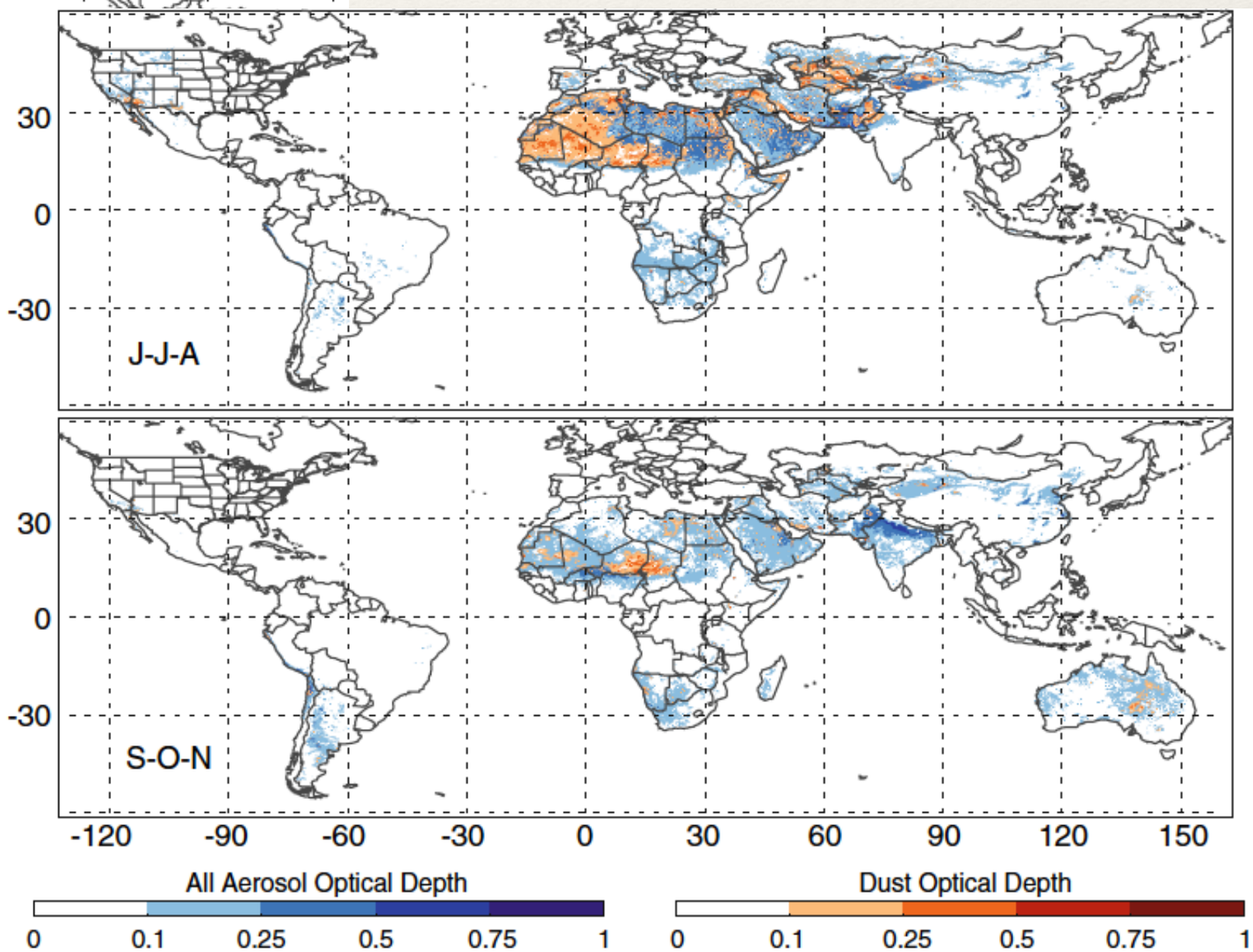

source regions: global data from polar-orbiting satellite ctd.

- interpretation of individual satellite dust products is complex
  - coarse res, transported vs. emitted?, restriction to clear sky conditions, contribution of other aerosol species
- Schepanski et al. [2012] highlight that differences in temporal res. among satellites is critical & conclude that different satellite methods lead to the identification of different source areas
- however, obs. from space are one of the most powerful tools to locate and study dust sources, particularly in combination w/numerical models [Hunees et al. 2012; Ginoux et al. 2012]

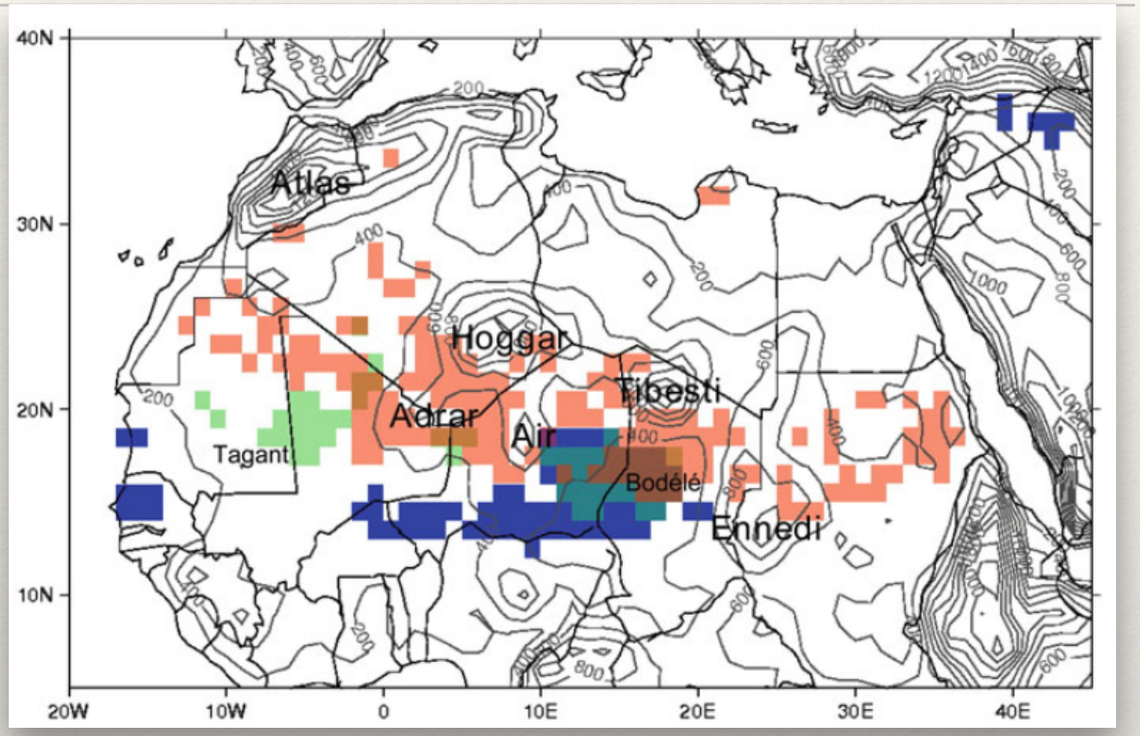

Fig. 7.3 Summary of main dust source areas inferred from satellite observations. Different colours indicate the three satellite dust products: blue MODIS Deep Blue AOD frequency >40 %, green OMI AI frequency >40 % and red MSG dust source activation frequency >6 %. Contour lines represent topography and are given at 200 m intervals. The figure illustrates the differences between the three satellite datasets in terms of identification of dust source regions (except for the Bodélé Depression) (From Schepanski et al. 2012)

7.3.2 Transport, general features

- possible to apply satellite obs. to track long-range transport of desert dust
  - some studies go beyond simple detection imagery to try to quantify dust transport (e.g., estimate columnar mass transport of desert dust [Dulac et al. 1992; Kaufman et al. 2005])
  - trans-Atlantic transport well-documented, but not trans-Pacific
    - using satellites to understand dust transport in SH requires more ground-level obs.
    - using satellites to examine dust events over Alaska, New Zealand, & Iceland is of primary interest
- high variability of dust transport in space and time (diurnal, seasonal, multi-annual) revealed by ground- and space- based observations
  - main drivers are met. factors (impact both emission & transport)
- primarily, investigation of transport has been transport from the largest dust source, N. Africa, and to the dominant direction of export from N. Africa, the N. tropical Atlantic

POLDER can partition coarse mode into spherical + non-spherical components [Herman et al. 2005]

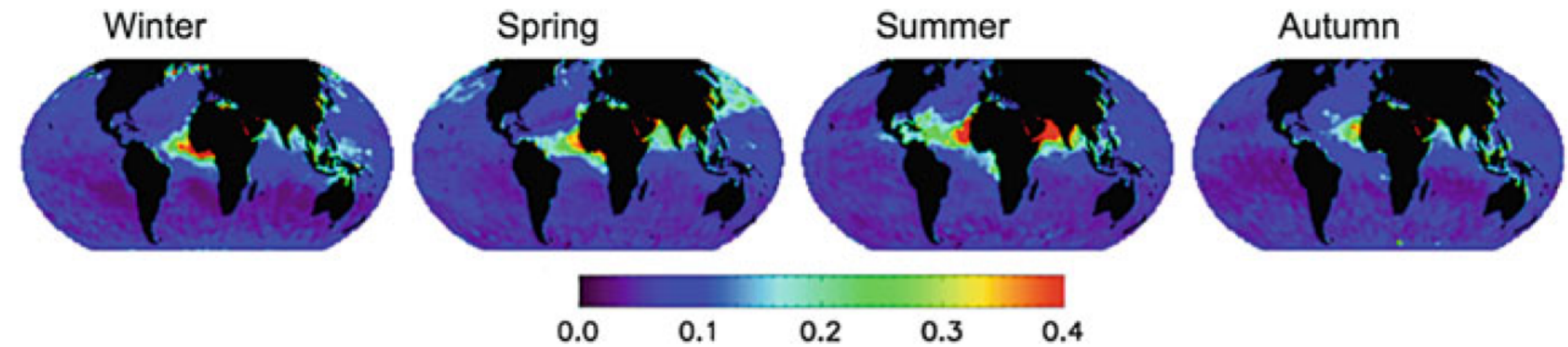

Fig. 7.4 Seasonal distribution of POLDER-3 AOD of the nonspherical coarse mode at 550 nm over oceans for the year 2009. Seasons are ordered from the *left* to the *right* (winter, spring, summer, autumn, respectively) (From Tanré et al. 2011)

most widespread and intense transported dust plumes occur during summer from Saudi Arabia and the Sahara; lowest dust loads occur during autumn

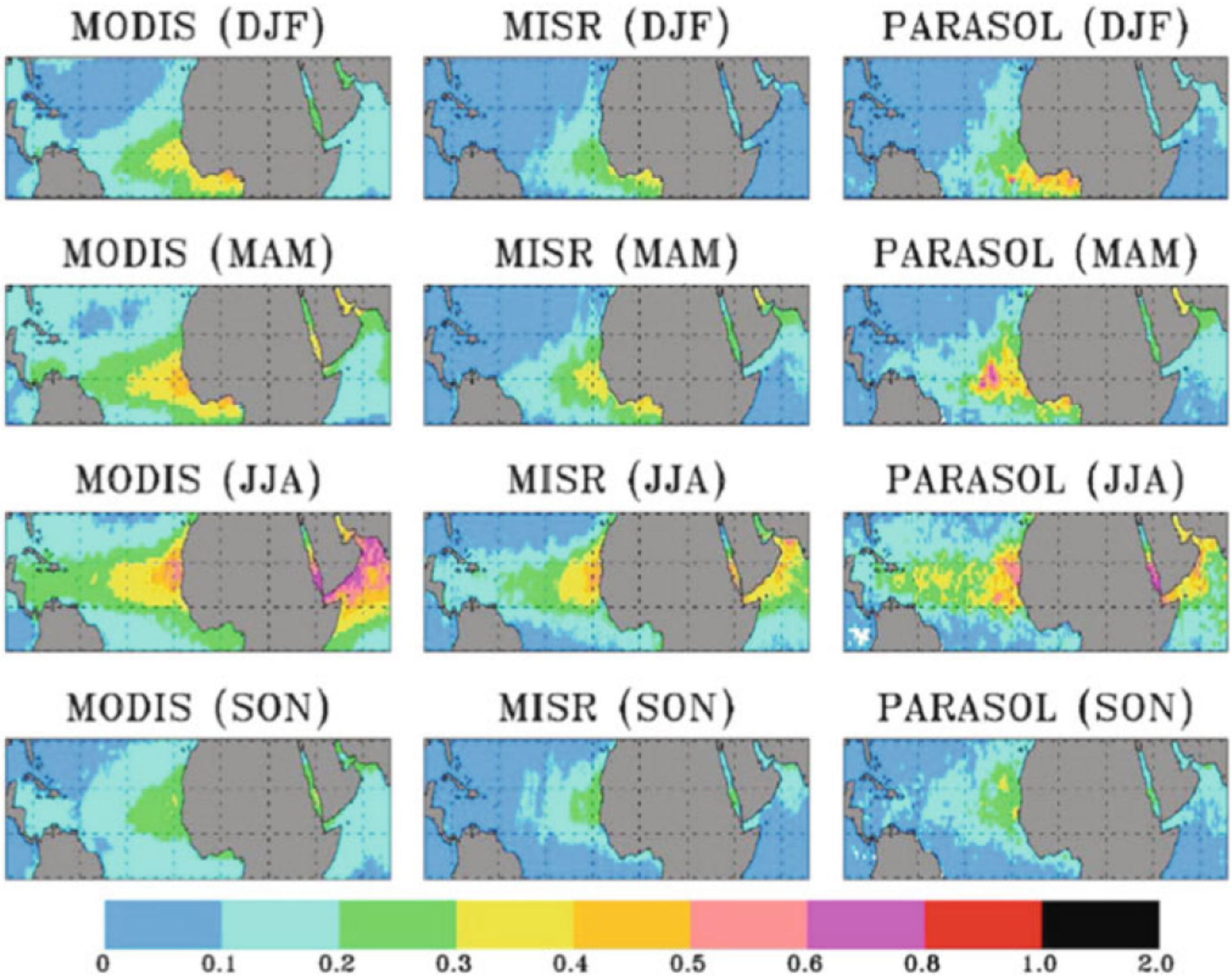

Fig. 7.5 Seasonal variations of trans-Atlantic dust transport. Shown are season-mean dust AODs as seen by MODIS, MISR and PARASOL. Each sensor applies a specific algorithm or methodology to discern dust from the total aerosol signal (From Yu et al. 2013)

recent developments in satellites + dust

- combining info. from different satellite sensors such as MODIS and MISR valuable to look at evolution of dust properties during transport, & to increase coverage [Kalashnikova and Kahn 2008]
- use daytime polar-orbiting satellite data w/ new gen. of high-res. IR spectrometers & interferometers (these get dust @ night)
- new DOD retrieval from IASI for dust obs. @ night & day [Klüser et al. 2011]
- dust altitude and effective particle size from AIRS [Pierangelo et al. 2004; DeSouza-Machado et al. 2010; Peyridieu et al. 2010]

until recently satellite dust obs. limited to clear sky cond'ns

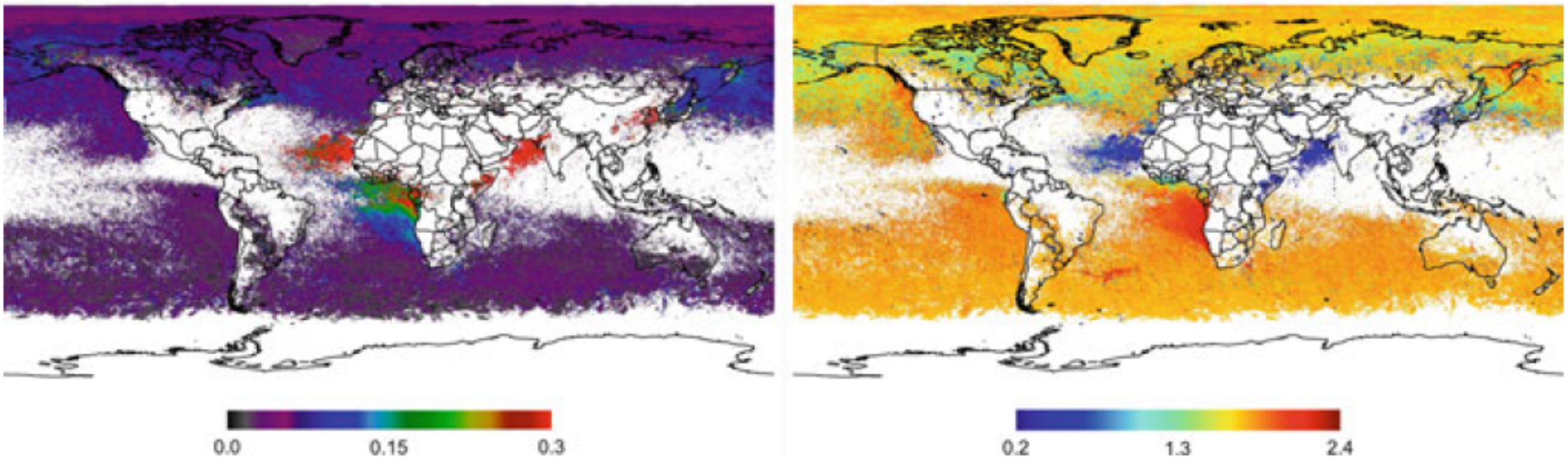

Fig. 7.6 Global mean AOD at 865 nm (*left*), mean Angström exponent (*right*) retrieved over clouds from POLDER-3 in summer 2009 (Courtesy of Peers and Waquet)

- mineral dust aerosols, associated w/low Angström exponents & high AOD, detectable over "dust belt"
- mean AOD (over dust belt?) at 865 nm is 0.456 <= lower limit b/c optically thick cloud below this

takeaway: dust transported above clouds is significant at a global scale

7.3.3. iav & trends

visibility data collected at met. stations present the long time series available but potential biases in these time series requires special attention [Mahowald et al. 2007]

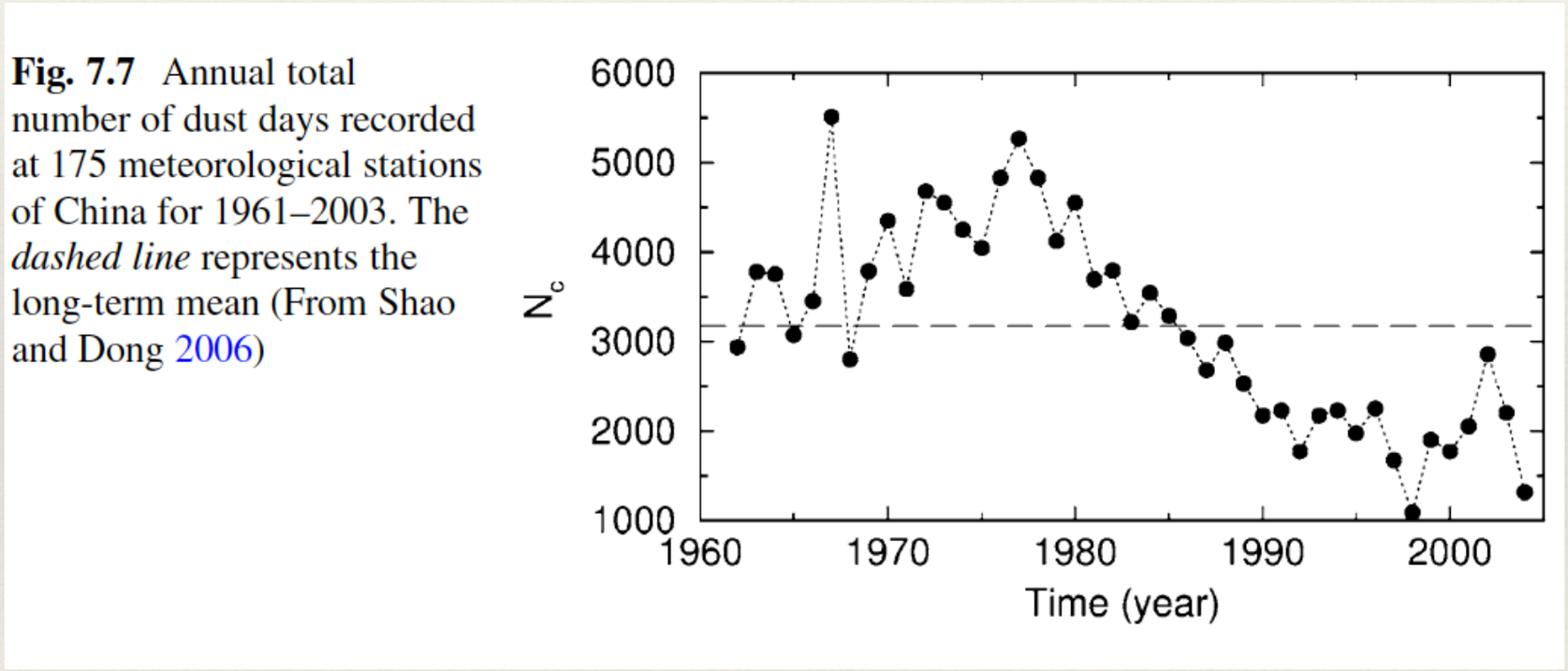

Fig. 7.7 Annual total number of dust days recorded at 175 meteorological stations of China for 1961–2003. The *dashed line* represents the long-term mean (From Shao and Dong 2006)

- marked decrease in late 1970s and 1980s, then clear negative trend until 1997
- interestingly, this trend is not observed in annual variations of dust-event days in transport-affected regions (e.g., Japan [Kurosaki and Mikami 2003])

substantial progress in understanding dust over periods > 10 years thanks to satellite obs.

- NAO shown to be a control on IAV in dust over N. Atlantic Ocean and Mediterranean Sea [Moulin et al. 1997] based on 11 years of Meteosate obs. of dust transport out of N. Africa
- large regional impact of Sahel drought cond'ns on IAV of dust transport over Atlantic in summer & winter using Barbados (1966-200) + TOMS + Meteosat over tropical N. Atlantic [Chiapello et al. 2005]; NAO influence restricted here to winter
- Azores High most important control on dust IAV during winter in 23 years of TOMS [Riemer et al. 2006]
- quantity of N. African dust over Caribbean and length of dust season increased during 1980s and plateaued during 1990s, using TOMS/Nimbus 7 and TOMS/Earth Probe [Doherty et al. 2008]
- decreasing trend in Atlantic dustiness from 1984-2008 [Evan and Mukhopadhyay; Foltz and McPhaden 2008]
  - most likely explanation is significant increase in rainfall over Sahel since mid-1980s

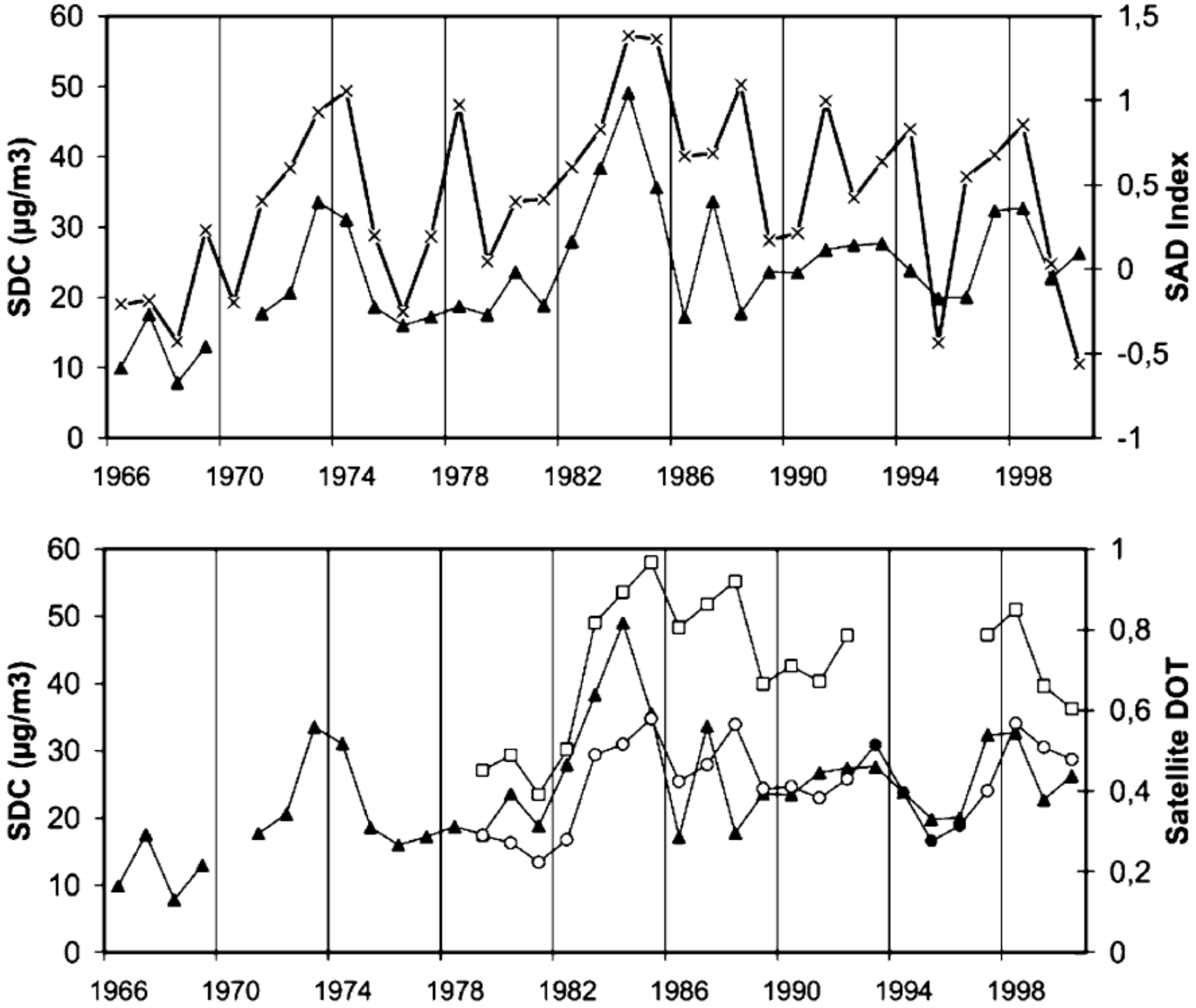

Fig. 7.8 *Top*: time series of summer mean Barbados surface dust concentrations (*solid triangles*) along with the Sahelian Annual Drought Index (*crosses*) from 1966 to 2000. *Bottom*: time series of summer mean Barbados surface dust concentrations (*solid triangles*) and summer mean satellite DOD over the tropical North Atlantic (15–30°N, *open circles* from TOMS, *shaded circles* from Meteosat/VIS) and over the Sahel (15–17°N, *squares*) (From Chiapello et al. 2005)

however, important to note that its difficult to demonstrate direct causal relationships b/w atmospheric indices (e.g., NAO, rainfall in Sahel) and multiannual evolution of dust transport. furthermore mechanisms not fully understand

7.3.4 vertical structure

- recent development & advancements lidar (light detection and ranging) techniques provide unprecedented view of vertical structure of mineral dust distribution
- ground-based networks, field campaigns & CALIOP on CALIPSO satellite

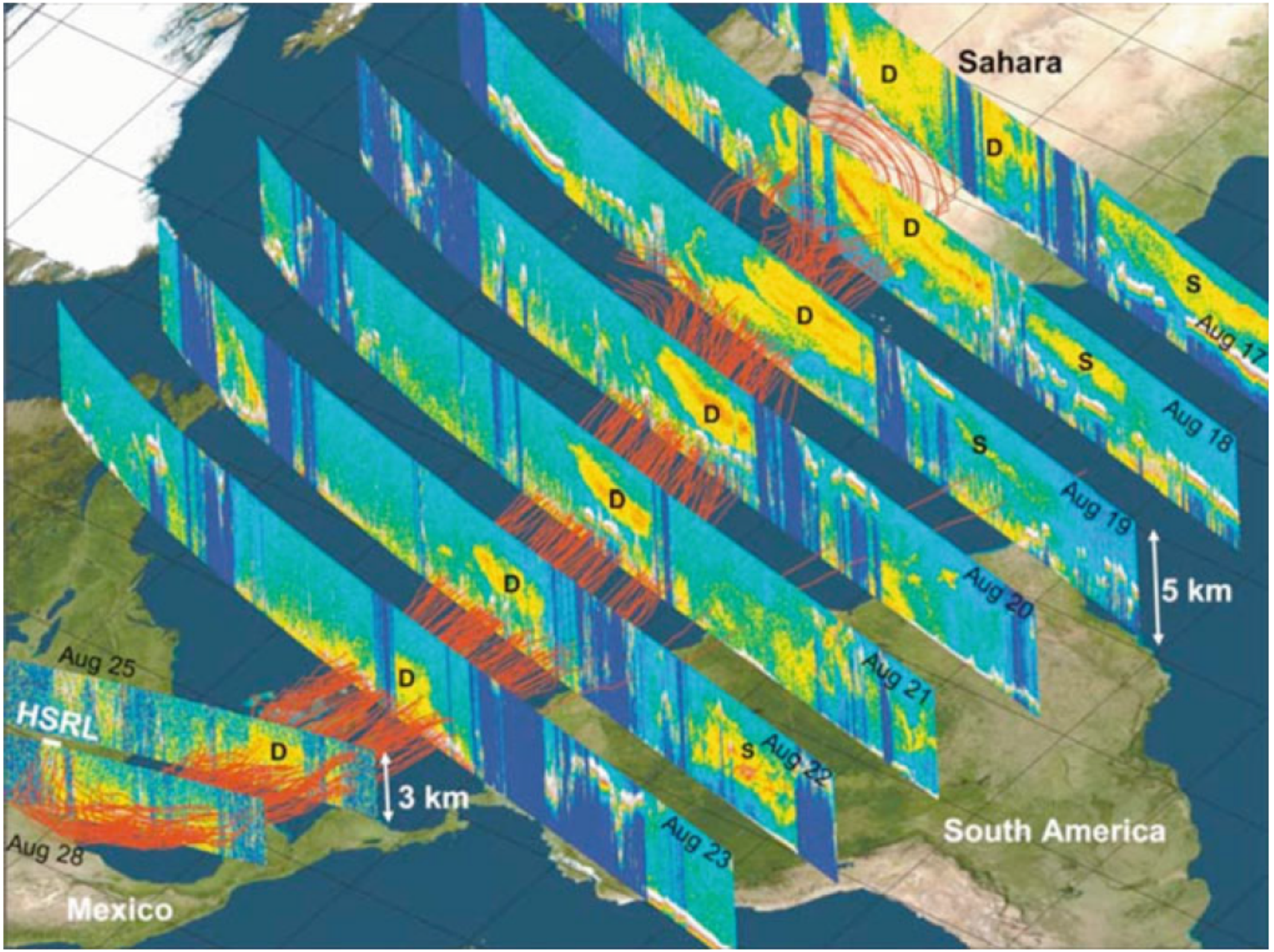

Fig. 7.9 An example demonstrating the capability of CALIOP to track dust long-range transport during a dust event that originated in the Sahara desert on 17 August 2007 and was transported to the Gulf of Mexico. Vertical images are 532-nm attenuated backscatter coefficients measured by CALIOP when passing over the dust transport track (From Liu et al. 2008a)

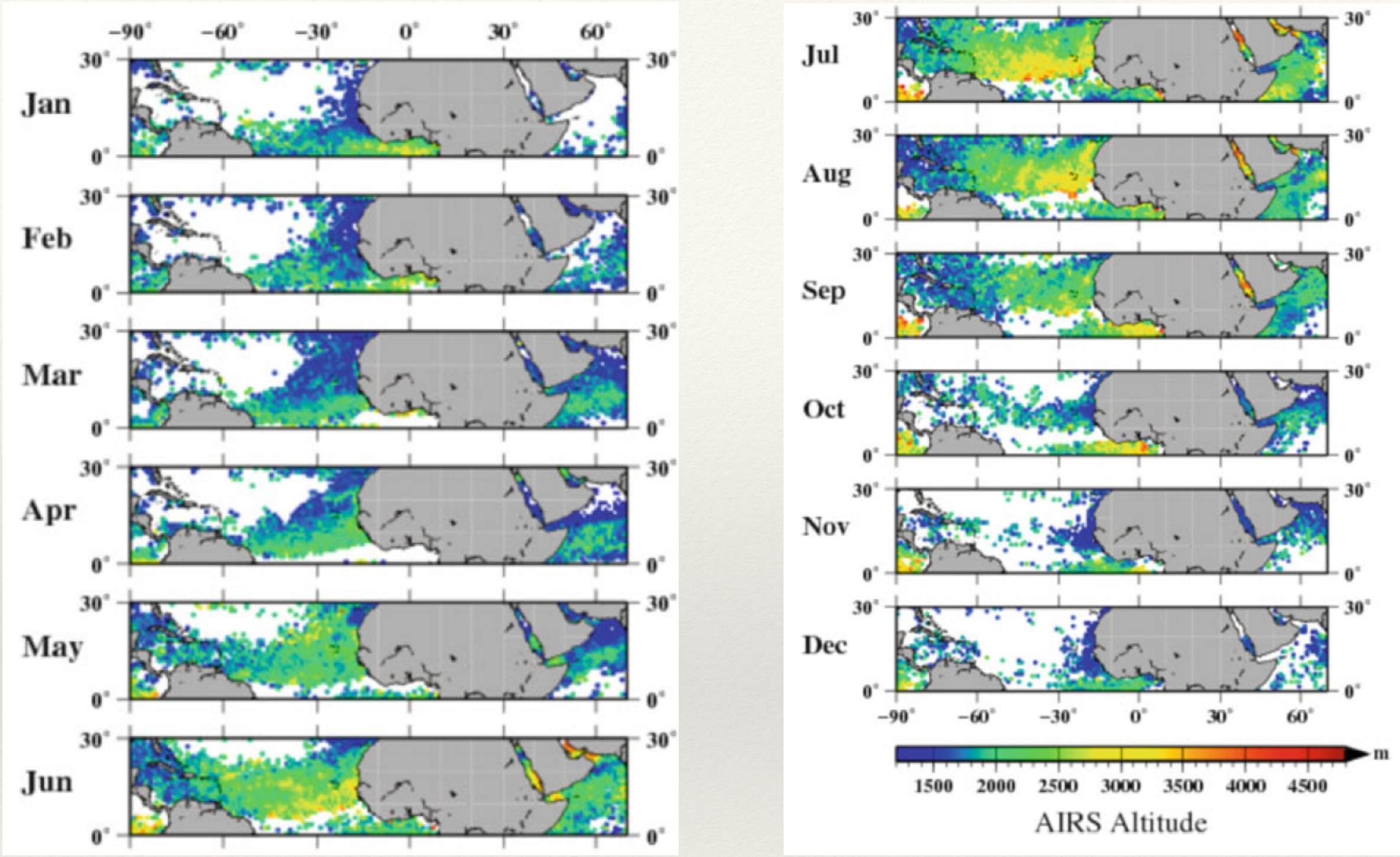

Fig. 7.10 Monthly climatology (1° x 1° resolution) of the aerosol layer mean altitude retrieved by AIRS over the period 2003–2008 (From Peyridieu et al. 2010)

Atmos. Chem. Phys., 14, 13043–13061, 2014
www.atmos-chem-phys.net/14/13043/2014/
doi:10.5194/acp-14-13043-2014

Atmospheric Chemistry and Physics Open Access

An improved dust emission model – Part 2: Evaluation in the Community Earth System Model, with implications for the use of dust source functions

J. F. Kok[1], S. Albani[2], N. M. Mahowald[2], and D. S. Ward[2]

"Unfortunately an accurate quantification of dust interactions w. the Earth system in past and future climates in hindered by the empirical nature of dust emission parameterizations in climate models."

- parameterizations tuned to reproduce current dust cycle [Ginoux et al. 2001; Zender et al., 2003a; Cakmur et al., 2006]

1. intro

- many dust modules in climate models use a dust source function S [Ginoux et al. 2001; Tegen et al. 2002; Zender et al. 2003b, Grini et al. 2005; Koven and Fung 2008] to account for global variation in "soil erodibility"
- need for a source function noted by [Ginoux et al. 2001]: co-location of dust "hot spots" & topographic depressions
  - design source function based on relative height of a model grid cell compared to surrounding cells
  - some subsequent studies challenged association of "hot spots" & top. dep.

$$\phi_d = C_{tune}\, S\, F_d$$

Take-aways

- use of S & consequent shift of emissions to regions w/ high obs. dust loadings can substantially improve modeled present-day dust cycle
  - this suggests that a key piece of physics is missing
- using empirical parameterizations and S will not allow for accurate model simulation of climate effects on soil erodibility, possibly leading to substantial errors when looking at previous and future climate

I. intro: summary of Kok et al. 2014a

- objective of both Kok et al. [2014] papers: step towards an improved representation of the global dust cycle in climate models, particularly for climate regimes other than the current climate (to which most models are tuned)
- Kok et al. 2014a present physically based theory for Fd emitted by an eroding soil (K14)
  - reproduce QC'd dust flux measurements w/ substantially less error than existing parameterizations
  - relatively straightforward to implement b/c only uses globally available parameters
- critical insight from Kok et al. 2014a: Fd likely substantially more sensitive to changes in soil state than most climate models account for (this supports why we needed a source function in the first place)
  - => hypothesis: if we have improved the sensitivity in K14, then having a source function will be less important

1. intro: objective of Kok et al. 2014b

- use CESM (v1.1) simulations to test this hypothesis, and evaluate performance of K14 in a climate model
  - 1) describe CESM dust module and implementation of K14 and measurements used to evaluate CESM dust cycle sims
    - 4 different combinations of S and Fd parameterizations (Table 1)
    - AERONET AOD, satellite DOD & dust mass path (DMP), ground measurements from source regions (dust surface concentration and dust deposition)
  - 2) present results and discuss implications of model eval.

coupling b/w land & atm. models in climate model

- emissions of dust aerosols in CESM simulated in its land model CLM4
- emissions then used by CESM's atmospheric model CAM4 to calculate 3D transport & deposition & DOD

2.1.1 general treatment of the dust cycle in CESM

$$\phi_d = C_{tune}\, S\, F_d$$

- emission of dust aerosols in CLM follows Zender et al. [2003a], Mahowald et al. [2006b, 2010]

2.1.1 general treatment of the dust cycle in CESM

$$\frac{u'_{*t}}{u'_{*dt}} = 1, (w < w'), \qquad \text{Fecan et al. 1999} \qquad (2)$$

$$\frac{u'_{*t}}{u'_{*dt}} = \sqrt{1 + 1.21(w - w')^{0.68}}, (w \geq w'), \qquad (3)$$

where u'_{*t} and u'_{*dt} are respectively the threshold friction velocities in the presence and absence of soil moisture, and u'_{*dt} is calculated following the semiempirical relation of Iversen and White (1982), as described on p. 3 of Zender et al. (2003a). Furthermore, w is the gravimetric water content in percent for CLM4's top soil layer, which has a thickness of 1.75 cm (Oleson et al., 2010). The threshold gravimetric water content w' of the top soil layer above which w increases u'_{*t} is given by (Fecan et al., 1999; Zender et al., 2003a)

$$w' = b\left(17 f_{clay} + 14 f_{clay}^2\right), \qquad (4)$$

where w' is given in percent, b is a tuning parameter introduced by Zender et al. (2003a), and f_{clay} is the soil's clay fraction, which is taken from the FAO (2012) soil database

- the larger b => smaller effect of soil moisture on dust emission threshold u'_{*t}
- choice of b important; ranges from <1, 3, $1/f_{clay}$
- "correct" b is highly uncertain (eq. 2 & 3 are based on wind tunnel studies) and likely depends substantially on model methodology, in particular model's hydrology module
- this paper runs sims for many choices of b, finding the best overall results for b=1 (authors note that modelers w/ other climate models should also try many values of b before settling)

2.1.1 general treatment of the dust cycle in CESM

- CLM4 accounts for inhibition of dust emissions by veg.
  - f_{bare} decreases linearly with LAI; no dust emission above LAI = 0.3 [Mahowald et al. 2010]
  - Ginoux et al. [2001] S already accounts for veg.
- CAM4 distributes emitted dust from CLM4 into four size bins [Mahowald et al. 2006b] following "brittle fragmentation" dust size distrib. [Kok 2011b]
  - emitted dust size distrib. does not depend on wspd (in agreement w/ obs. [Kok 2011b])
  - optical properties for each bin, derived from representation of dust as internal mixture of primary mineral classes of dust (quartz, aluminosilicates, clays, carbonates, iron-bearing minerals) combined into an effective medium using Maxwell Garnett approx. [Albani et al. 2014]
- CAM4 has both dry and wet deposition of dust (next week?)

Simulation	Dust flux	Dust source function
I "control"	Zender et al. (2003a)	None
II	Zender et al. (2003a)	Zender et al. (2003b)
III	Zender et al. (2003a)	Ginoux et al. (2001)
IV	Kok et al. (2014)	None

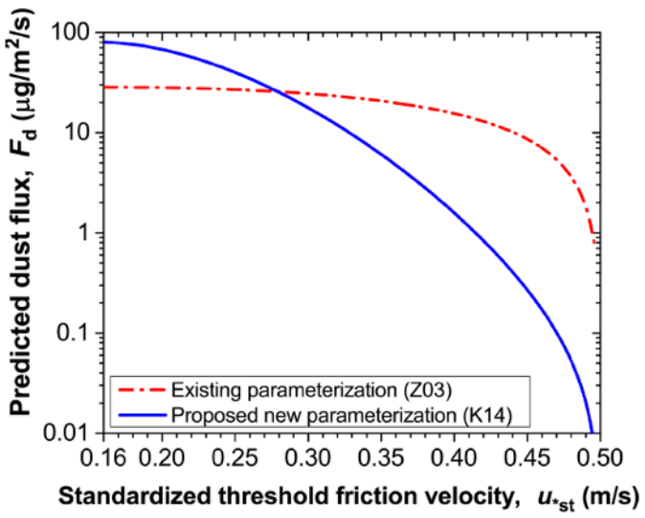

Figure 1. The vertical dust flux (F_d) as a function of the soil's standardized threshold friction velocity (u_{*st}) in CESM for the default Z03 dust flux parameterization (Eq. 6; dash-dotted red line), and for the K14 parameterization (Eq. 7; solid blue line). Results are shown for $u_* = 0.50\ \mathrm{m\ s^{-1}}$ and for $f_{clay} = 15\ \%$, which is a typical value for dust emitting regions (see Fig. S1 in the Supplement). The predicted dust fluxes include the global tuning factors that eliminate the bias against AERONET AOD measurements for simulations I and IV, respectively (see Eq. 1 and Sect. 2.2.1).

F_d substantially more sensitive to soil's threshold friction velocity in K14 than Z03, in agreement w/ obs.

$$\phi_d = C_{tune}\, S\, F_d$$

Zender et al. 2003a "Z03"

$$F_d = C_{MB}\,\eta\, f_{bare}\,\frac{\rho_a}{g}\,u'^3_*\left(1-\frac{u'^2_{*t}}{u'^2_*}\right)\left(1+\frac{u'_{*t}}{u'_*}\right), \qquad (6)$$

$$\left(u'_* > u'_{*t}\right),$$

Kok et al. 2014 "K14"

$$F_d = C_d\, f_{bare}\, f_{clay}\,\frac{\rho_a\left(u_*^2-u_{*t}^2\right)}{u_{*st}}\left(\frac{u_*}{u_{*t}}\right)^{C_\alpha\frac{u_{*st}-u_{*st0}}{u_{*st0}}}, \qquad (7a)$$

$$\left(u_* > u_{*t}\right).$$

$$C_d = C_{d0}\exp\left(-C_e\frac{u_{*st}-u_{*st0}}{u_{*st0}}\right). \qquad (7b)$$

2.2.1 AERONET AOD

- daily averaged level 2.0 QA AOD (pre & post field calibrated & manually inspected), obtained from v2 direct sun algorithm
- select “dusty” AERONET stations to evaluate model vs. AERONET
  - find “dusty” stations using model
    - grid box over a station in model sims needs to indicate >50% annual mean AOD is from dust aerosol
    - for each station, only select days w/ Angstrom exp. in 440-870 nm < 1 (meaning the aerosols are coarse and mostly likely to be dust)
  - comparisons between AERONET & model are sensitive to C_{tune}, which scales the global dust cycle
    - C_{tune} is poorly constrained [Cakmur et al. 2006; Hunees et al. 2011] so authors select a value for each of the 4 sims st. the bias is reduced
- compare models vs. AERONET on daily, seasonal, and climatological (i.e., 1995-2011) timescales

2.2.2. Satellite-derived estimates of DMP

- use DOD & DMP (g/m^2) off the coast of W. Africa around Cape Verde [Evan et al. 2014] as additional tests of dust emission component of CESM
- one unit of dust AOD = 2.7 +/- 0.4 g/m^2 of suspended dust [Kaufman et al. 2005]

2.3.1 surface concentration measurements

- N. Atlantic (AEROCE) [Arimoto et al. 1995]
- Pacific Ocean (SEAREX) [Prospero et al. 1989]
- look at 15 stations (only use stations in CESM that have at least some dust)
- compare climatological seasonal cycles b/w model + obs. for each station (note that time frame of obs. is different from model 1995-2011)

2.3.2 deposition measurements

- 110 stations compiled by Albani et al. [2014];
  - only measurements representative of modern climate
  - size range of the measured deposition flux adjusted to be consistent w/ dust size range in CESM
- only can compare measured annual deposition flux at each station against that simulated by CESM (b/c deposition fluxes represent integration over years to decades, evaluation of simulated daily to seasonal variability is not possible w/ these measurements)
  - dates don't line up - so look at annual observed deposition flux against simulated climatological mean annual deposition flux

$$\phi_d = C_{tune}\, S\, F_d$$

Kok et al. 2014 "K14"

$$F_{\mathrm{d}} = C_{\mathrm{d}}\, f_{\mathrm{bare}}\, f_{\mathrm{clay}}\, \frac{\rho_{\mathrm{a}}\left(u_*^2 - u_{*\mathrm{t}}^2\right)}{u_{*\mathrm{st}}} \left(\frac{u_*}{u_{*\mathrm{t}}}\right)^{C_\alpha \frac{u_{*\mathrm{st}} - u_{*\mathrm{st0}}}{u_{*\mathrm{st0}}}}, \qquad (7a)$$

$$(u_* > u_{*\mathrm{t}}).$$

$$C_{\mathrm{d}} = C_{\mathrm{d0}} \exp\left(-C_{\mathrm{e}} \frac{u_{*\mathrm{st}} - u_{*\mathrm{st0}}}{u_{*\mathrm{st0}}}\right). \qquad (7b)$$

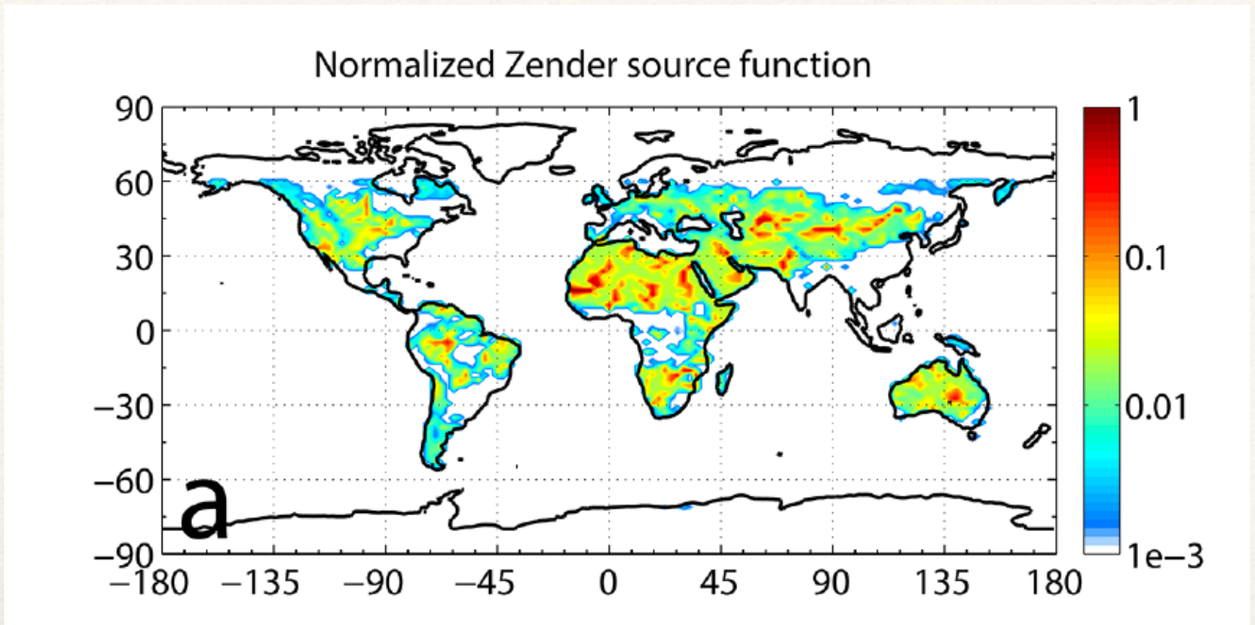

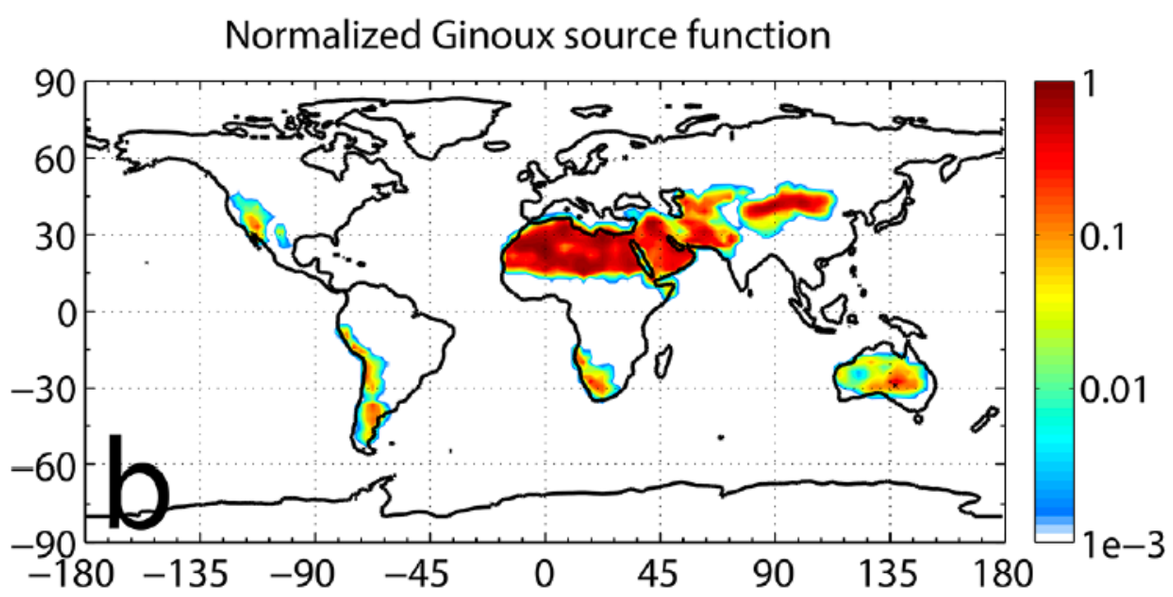

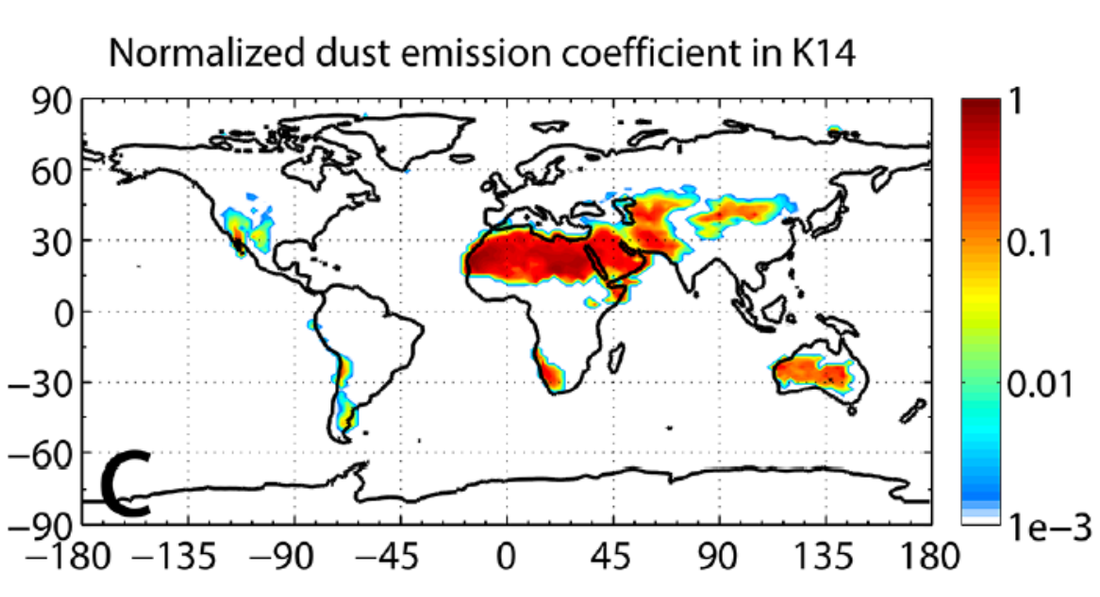

Figure 2. Global maps of **(a)** the Zender et al. (2003b) geomorphic source function used in simulation II, **(b)** the Ginoux et al. (2001) source function used in simulation III, and **(c)** the K14 dust emission coefficient C_{d} (see Eq. 7b), averaged over the model run (1995–2011). The seasonal cycle of C_{d} is reported in Fig. S3 in the Supplement. Since the Ginoux et al. (2001) source function inherently includes the fraction of the grid cell that consists of bare soil, both the Zender et al. (2003b) source function and the dust emission coefficient C_{d} were multiplied by the grid cell's bare soil fraction (see Eq. 5). To further facilitate comparison, the source functions and C_{d} are each normalized by their highest occurrence in any of the grid boxes.

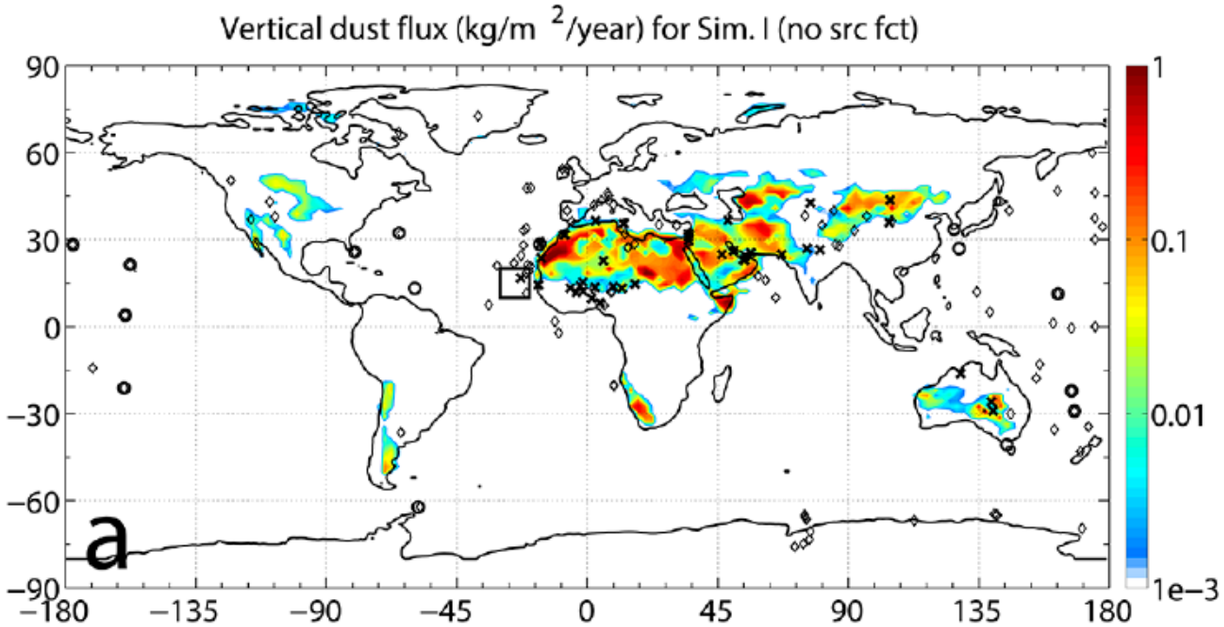

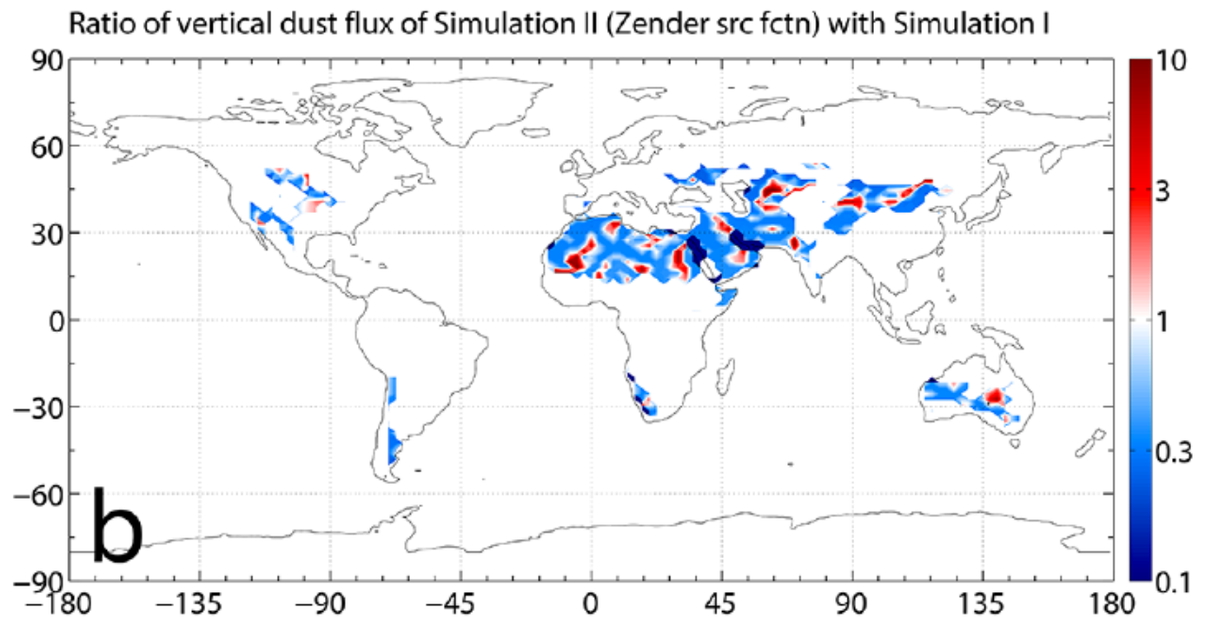

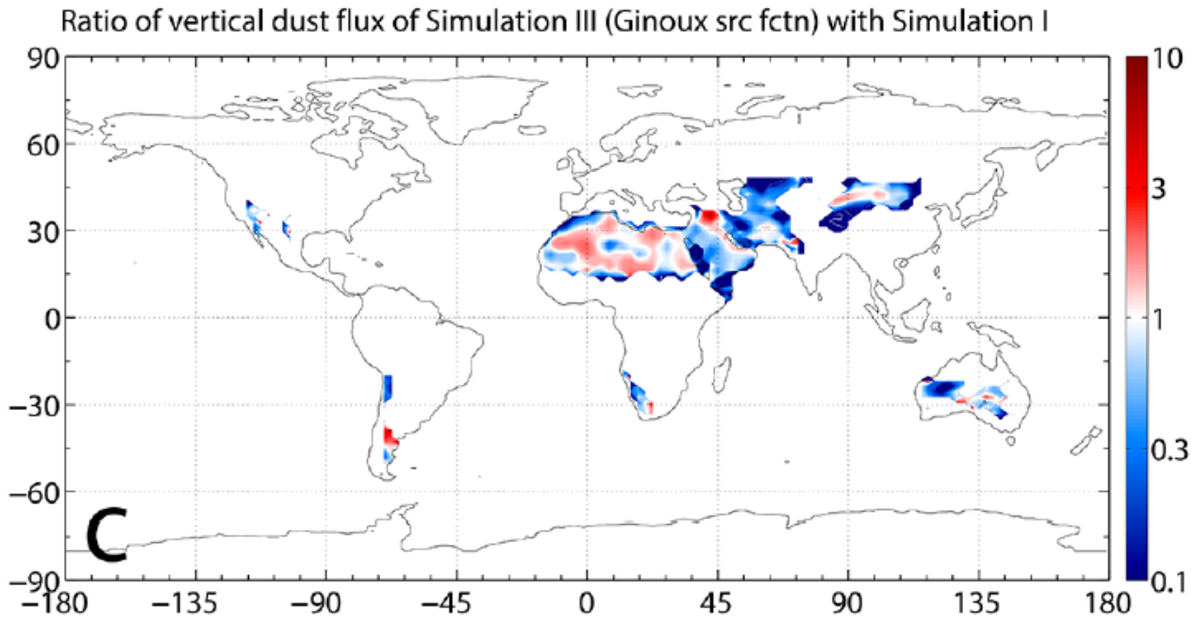

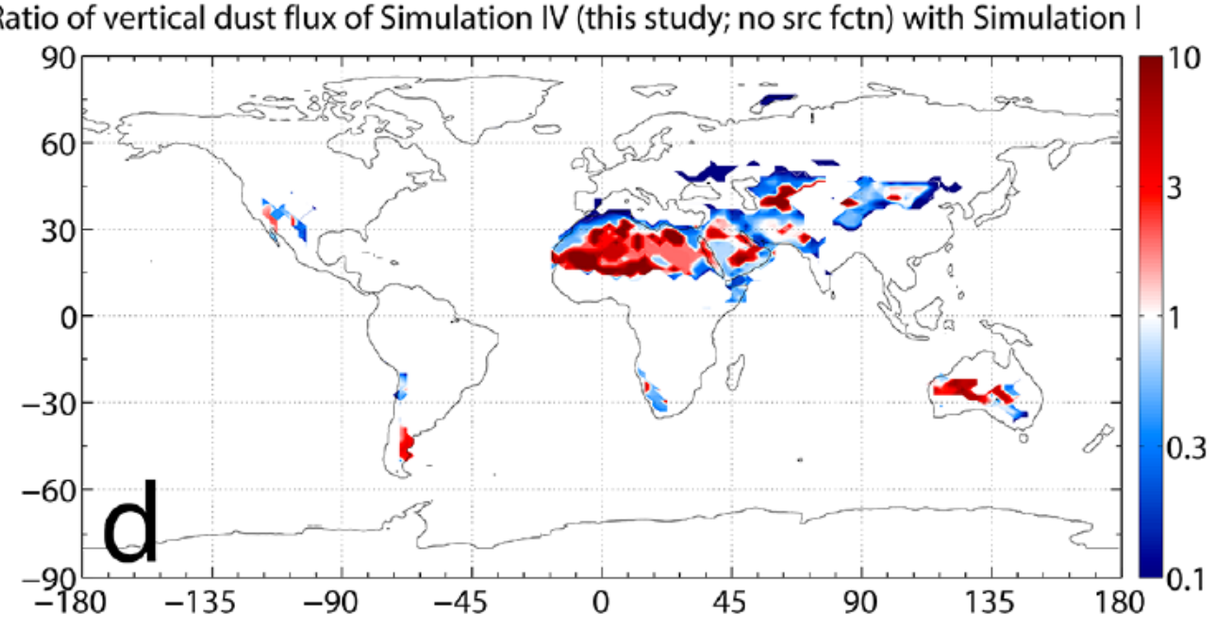

Figure 3. Global maps of **(a)** the simulated vertical dust flux for simulation I and **(b–d)** the ratios of the dust flux in simulations II–IV to the flux in simulation I. Red (blue) coloring in panels **(b–d)** denotes increases (decreases) in dust emission fluxes relative to the "control" (simulation I). In panel **(a)**, crosses, circles, and diamonds respectively mark the locations of measurements of AERONET AOD, dust surface concentration, and dust deposition flux. The square denotes the area off the coast of West Africa for which the satellite-derived dust AOD and DMP were used (Evan et al., 2014).

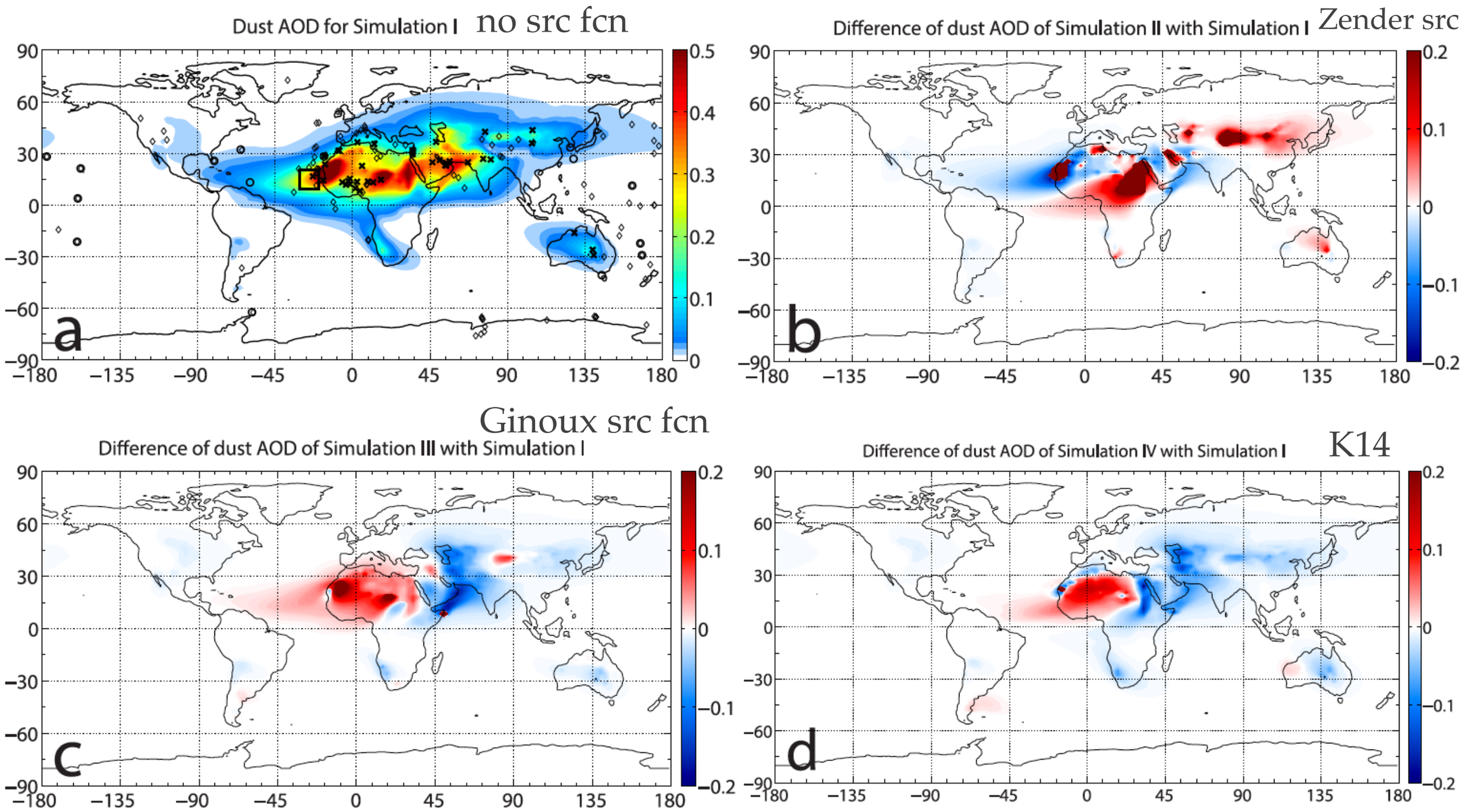

Figure 4. Global maps of **(a)** the dust AOD of simulation I, and **(b–d)** the difference of dust AOD from simulations II–IV with that of simulation I. Red shading denotes increases in dust AOD relative to the "control" (simulation I). Black symbols in panel **(a)** are as defined in Fig. 3.

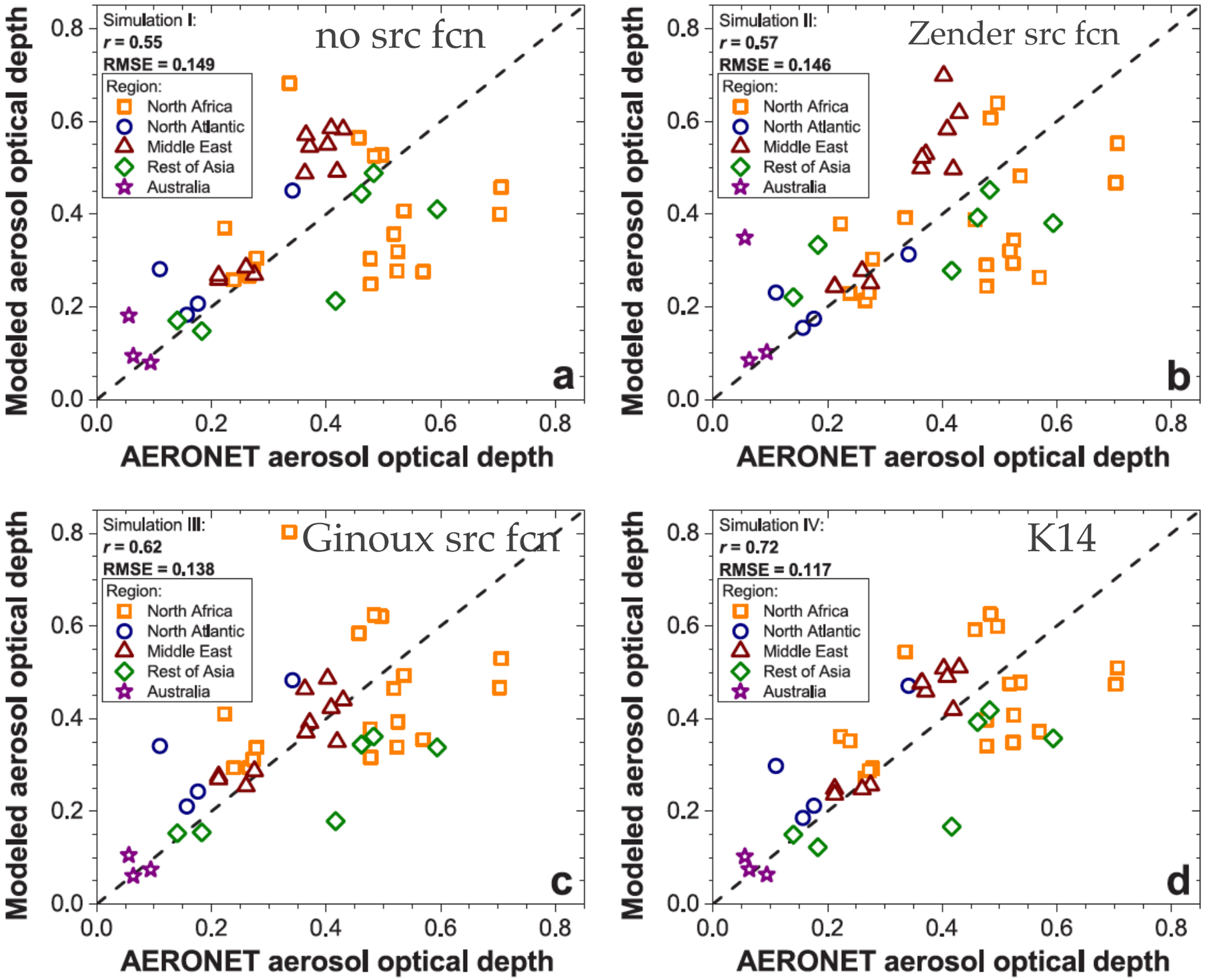

Figure 5. Comparison of measured and modeled AOD at 42 dust-dominated AERONET stations. Results are shown for **(a)** simulation I (no source function), **(b)** simulation II (Zender et al. (2003b) geomorphic source function), **(c)** simulation III (Ginoux et al. (2001) source function), and **(d)** simulation IV (no source function, and dust flux is parameterized following K14 instead of Z03). For each simulation, the RMSE and r are noted.

Table 1. Summary of the four CESM simulations used in this study, and the statistics of their comparisons against the data set most characteristic of dust emission, namely AERONET AOD measurements at dusty stations (see text). Model results are compared to measurements of AERONET AOD climatology (fourth and fifth columns), the mean correlation to the measured seasonal cycle at each station (sixth column), and the mean correlation to the measured daily variability at each station (seventh column). Statistically significant improvements (see Sect. 2.4) of simulations II–IV relative to the "control" simulation I are indicated with bold font. Additionally, simulation results that are statistically significantly improved over the results of each of the other three simulations are both bold and underlined.

Simulation	Dust flux parameterization	Dust source function	AERONET climatology, r	AERONET climatology, RMSE	AERONET seasonal cycle, r	AERONET daily variability, r
I	Zender et al. (2003a)	None	0.55	0.149	0.79	0.43
II	Zender et al. (2003a)	Zender et al. (2003b)	0.57	0.146	0.75	0.43
III	Zender et al. (2003a)	Ginoux et al. (2001)	0.62	0.138	0.79	0.42
IV	Kok et al. (2014)	None	**0.72**	**0.117**	**0.82**	**0.46**

- however, seasonal variability in AOD likely primarily controlled by seasonal variations in soil moisture, wind & vegetative soil cover => influence of emission scheme to improve seasonal variability of AOD is limited => r of sim 4 only slightly higher than other sims
- same thing goes for daily variability; emission scheme also has limited influence on daily variability, which is likely largely controlled by daily variability in wspd & soil moisture

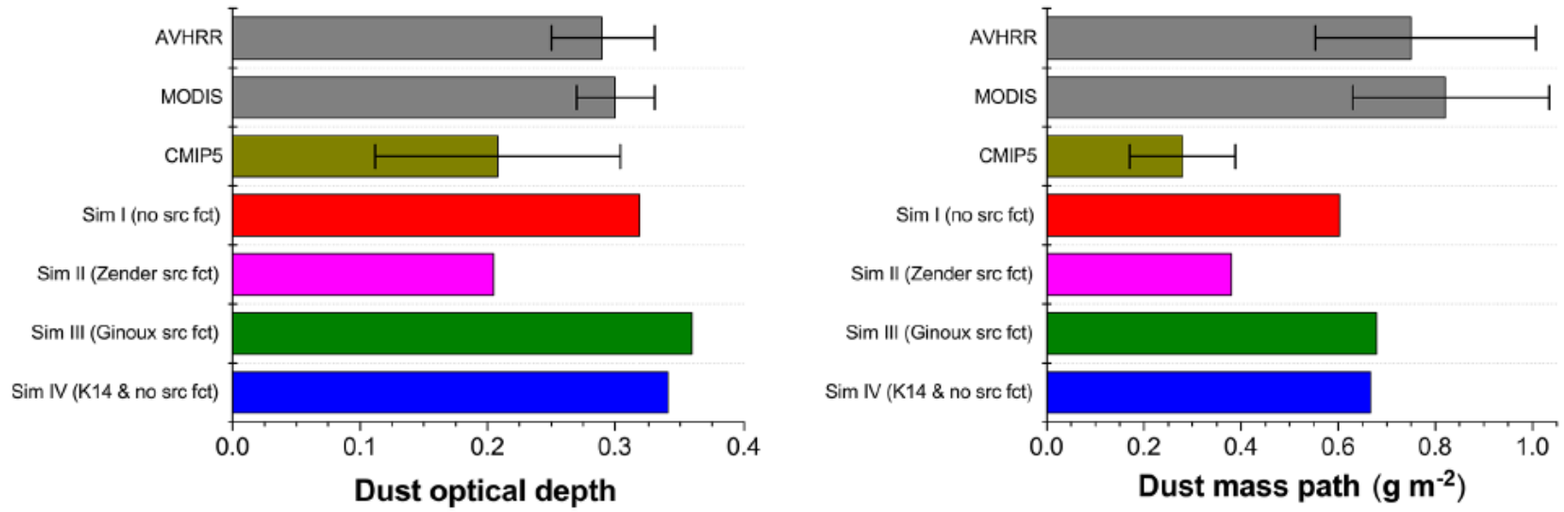

Figure 6. Dust optical depth (left) and dust mass path (right) averaged over the region 10–20° N and 20–30° W. Satellite-derived estimates for AVHRR (1982–2005) and MODIS (2001–2012), as well as the ensemble average of CMIP5 models (1982–2005), are from Evan et al. (2014). Error bars denote the uncertainty on the satellite estimates, and the standard deviation of the available CMIP5 model results (23 models for the dust optical depth, and 11 models for the dust mass path; see Evan et al., 2014). The dust optical depth and dust mass paths calculated from the four CESM simulations were averaged over the period 2001–2011 to be most comparable to the MODIS results.

Table 2. Statistics of the comparison of the four CESM simulations against data sets taken further from source regions, namely dust surface concentration measurements and dust deposition fluxes. Simulations and measurements are compared with respect to their climatology for both data sets and their seasonal cycle for the surface concentration. Statistically significant improvements (see Sect. 2.4) of simulations II–IV relative to the "control" simulation I are indicated with bold font. Additionally, simulation results that are statistically significantly improved over the results of each of the other three simulations are both bold and underlined.

Simulation	Dust flux	Dust source function	Surf. conc. climatology, r	Surf. conc. climatology, RMSE	Surf. conc. seasonal cycle, r	Dep. flux climatology, r	Dep. flux climatology, RMSE
I	Zender et al. (2003a)	None	0.92	0.32	0.62	0.79	0.88
II	Zender et al. (2003a)	Zender et al. (2003b)	0.88	0.42	0.61	**0.80**	**0.84**
III	Zender et al. (2003a)	Ginoux et al. (2001)	0.92	0.36	0.63	0.78	0.87
IV	Kok et al. (2014)	None	0.93	0.31	0.63	0.77	0.87

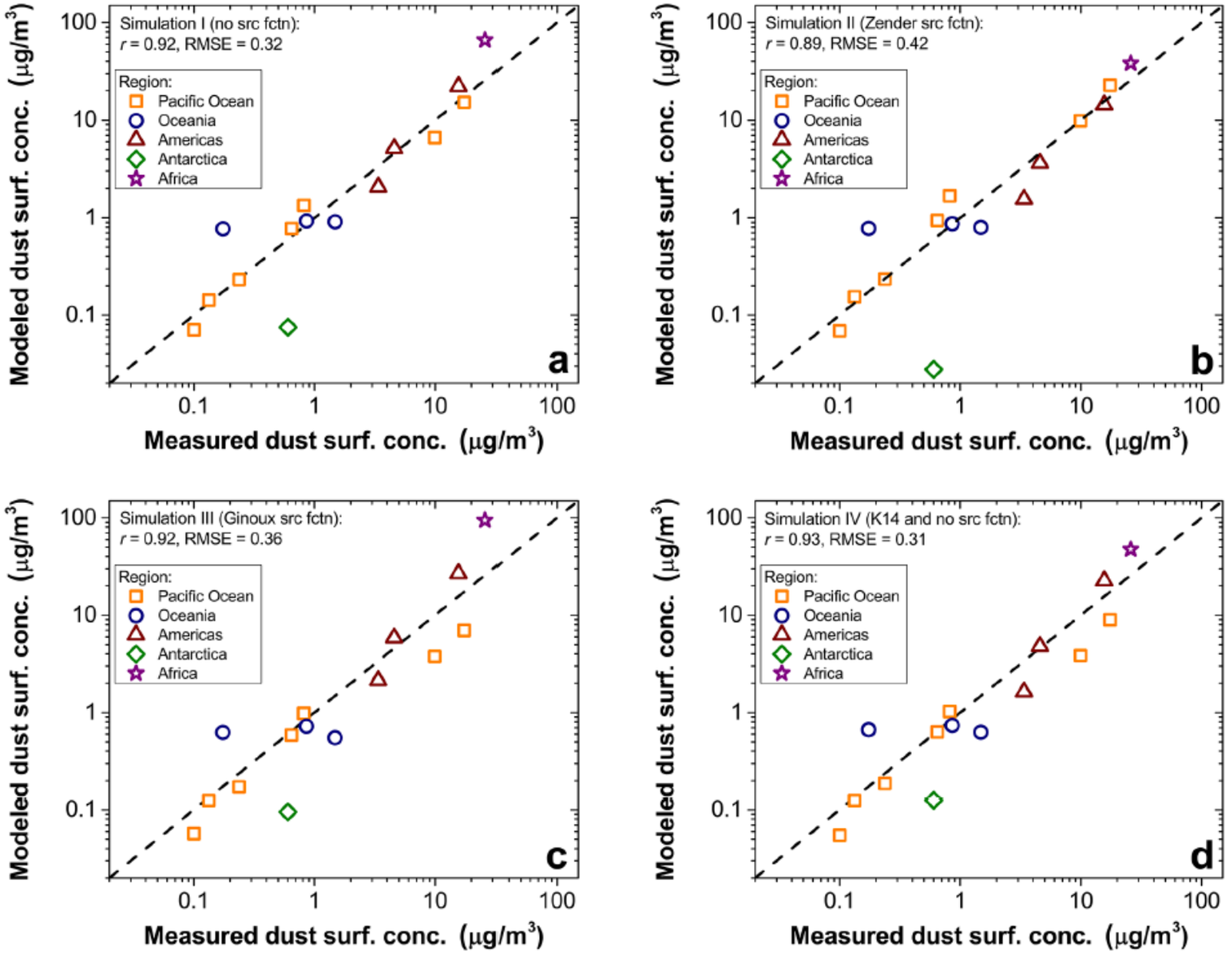

Figure 7. Comparison of the annually-averaged modeled dust surface concentration with that measured at 15 stations (see Sect. 2.3.1). Results are shown for **(a)** simulation I (no source function), **(b)** simulation II (Zender et al. (2003b) source function), **(c)** simulation III (Ginoux et al. (2001) source function), and **(d)** simulation IV (no source function, and dust flux is parameterized following K14 instead of Z03). For each panel, the RMSE and r in log10-space are noted.

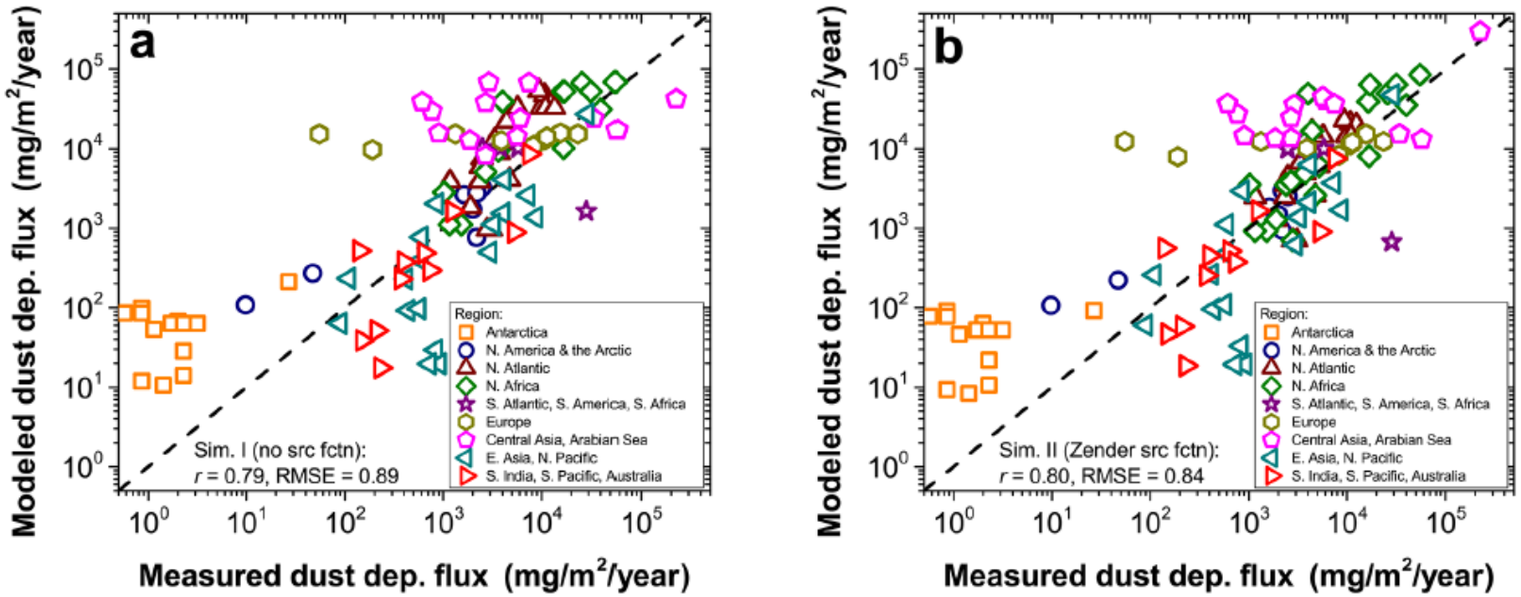

Figure 8. Comparison of the modeled dust deposition flux with that measured at 110 stations (see Sect. 2.3.2). Results are shown for **(a)** simulation I (no source function), **(b)** simulation II (Zender et al. (2003b) source function), **(c)** simulation III (Ginoux et al. (2001) source function), and **(d)** simulation IV (no source function, and dust flux is parameterized following K14 instead of Z03). For each panel, the RMSE and r in log10-space are noted.